

# Simultaneously Exposing and Jamming Covert Communications via Disco Reconfigurable Intelligent Surfaces

Huan Huang, *Member, IEEE*, Hongliang Zhang, *Member, IEEE*, Yi Cai, *Senior Member, IEEE*, Dusit Niyato, *Fellow, IEEE*, A. Lee Swindlehurst, *Fellow, IEEE*, and Zhu Han *Fellow, IEEE*

**Abstract**—Covert communications provide a stronger privacy protection than cryptography and physical-layer security (PLS). However, previous works on covert communications have implicitly assumed the validity of channel reciprocity, i.e., wireless channels remain constant or approximately constant during their coherence time. In this work, we investigate covert communications in the presence of a disco RIS (DRIS) deployed by the warden Willie, where the DRIS with random and time-varying reflective coefficients acts as a “disco ball”, introducing time-varying fully-passive jamming (FPJ). Consequently, the channel reciprocity assumption no longer holds. The DRIS not only jams the covert transmissions between Alice and Bob, but also decreases the error probabilities of Willie’s detections, without either Bob’s channel knowledge or additional jamming power. To quantify the impact of the DRIS on covert communications, we first design a detection rule for the warden Willie in the presence of time-varying FPJ introduced by the DRIS. Then, we define the detection error probabilities, i.e., the false alarm rate (FAR) and the missed detection rate (MDR), as the monitoring performance metrics for Willie’s detections, and the signal-to-jamming-plus-noise ratio (SJNR) as a communication performance metric for the covert transmissions between Alice and Bob. Based on the detection rule, we derive the detection threshold for the warden Willie to detect whether communications between Alice and Bob is ongoing, considering the time-varying DRIS-based FPJ. Moreover, we conduct theoretical analyses of the FAR and the MDR at the warden Willie, as well as SJNR at Bob, and then present unique properties of the DRIS-based FPJ in covert communications. We present numerical results to validate the derived theoretical analyses and evaluate the impact of DRIS on covert communications.

**Index Terms**—Covert communications, intelligent reflecting surface, signal detection, physical layer security, channel aging.

## I. INTRODUCTION

Due to the broadcast nature and superposition properties of wireless channels, wireless systems are inherently vulnerable to various malicious attacks [1]–[3]. This issue is particularly critical in the Internet-of-Things (IoT) era, where the data transmitted often contains sensitive personal information,

such as health and location data, and in scenarios involving government and military operations, where maintaining stealth is essential. As a result, research into transmission security and privacy has been advancing rapidly. Covert communications [4], also known as low probability of detection communications, aim to conceal the transmission’s existence from adversarial wardens by hiding the transmission within environmental noise [5], [6].

Covert communications offer a higher level of privacy protection compared to cryptography and physical-layer security (PLS) [7], [8] because the warden Willie will not attempt to decode the information contained in the signals if he is unaware of the transmission. In [5], the authors established a fundamental result in covert communications:  $o(\sqrt{n})$  bits can be sent in  $n$  additive white Gaussian noise (AWGN) channel uses while achieving an arbitrarily low probability of detection (LPD) without knowledge of the noise power on the channel between the transmitter Alice and the warden Willie, where  $o(\sqrt{n})$  represents a non-asymptotically tight upper bound on  $\sqrt{n}$ . Furthermore, if a lower bound on the noise power is known, up to  $\mathcal{O}(\sqrt{n})$  bits can be then sent, where  $\mathcal{O}(\sqrt{n})$  is an asymptotically tight upper bound on  $\sqrt{n}$ .

Following the work in [5], previous studies have introduced other techniques, such as non-orthogonal multiple access (NOMA) or Turbo encoding, to further enhance covert communications while guaranteeing transmission performance [9]–[11]. The works in [12]–[15] investigated the use of a jammer or adding artificial noise to further increase the power variation, thereby enhancing the difficulty of accurate decision-making by the warden Willie. In addition, [16], [17] demonstrated that the use of a relay can further increase power variations, thereby disrupting the warden Willie’s detection [18]. The authors of [19] proposed exploiting the variations in received power due to small scale fading in order to implement covert communications.

As summarized in Table I, the signals transmitted by Alice in covert communications can be effectively concealed from the warden Willie by uncertainty in the wireless communication channel, either due to inherent properties such as noise and fading, or factors introduced by Bob and Alice such as relays, coding, or jamming.

Recently, reconfigurable intelligent surfaces (RISs) have been considered as a critical technology to improve wireless communication performance [20]–[25]. These surfaces consist of numerous elements with reflective coefficients that can be adjusted using simple programmable PIN or varactor diodes [26]. The integration of RISs into wireless networks significantly enhances their performance without substantially

H. Huang and Y. Cai are with the School of Electronic and Information Engineering, Soochow University, Suzhou, Jiangsu 215006, China (e-mail: hhuang1799@gmail.com, yicai@ieee.org).

H. Zhang is with the State Key Laboratory of Advanced Optical Communication Systems and Networks, School of Electronics, Peking University, Beijing 100871, China (email: hongliang.zhang92@gmail.com).

D. Niyato is with the College of Computing and Data Science, Nanyang Technological University, Singapore 639798 (e-mail: dniyato@ntu.edu.sg).

A. L. Swindlehurst is with the Center for Pervasive Communications and Computing, University of California, Irvine, CA 92697, USA (e-mail: swindle@uci.edu).

Z. Han is with the Department of Electrical and Computer Engineering at the University of Houston, Houston, TX 77004 USA. (email: hanzhu22@gmail.com).

TABLE I  
COMPARISON OF COVERT COMMUNICATION IMPLEMENTATIONS

| Implementation           | Requirement            | Reference |
|--------------------------|------------------------|-----------|
| Environmental noise      | None                   | [5], [6]  |
| Path loss                | None                   | [19]      |
| Jamming/Artificial noise | Extra jamming power    | [12]–[15] |
| Relaying                 | Extra signal processes | [16]–[18] |

increasing power consumption or cost [27], [28]. The use of RISs in covert communications has already been explored in [29]–[33]. These studies have focused on exploiting one or more RISs for covert communications in systems employing NOMA [29], artificial noise [30], finite blocklength coding with variable prior probabilities [31], or unmanned aerial vehicles [32], [33].

All existing works on covert communications, with or without RISs, assume that channel reciprocity in time-division duplex (TDD) wireless channels either holds or is approximately valid. While such an assumption is normally reasonable, channel reciprocity can be broken in the presence of time-varying “Disco” RIS (DRIS) [34] or RIS employing non-reciprocal connections between their elements [35]. The concept using DRISs to launch fully-passive jamming (FPJ) attacks without relying on either channel knowledge of legitimate users or additional jamming power was further developed in [36]. The DRIS coefficients are time-varying and random, acting like a “disco ball”. Consequently, active channel aging (ACA) is introduced, invalidating the channel reciprocity of TDD channels even within the channel coherence time [37], [38]. Some works have also exploited DIRSs to disrupt key consistency in channel reciprocity-based key generation [39].

In this work, we investigate the novel concept of using DRISs to disrupt channel reciprocity in covert communications. The main contributions are summarized as follows:

- We first present the model of covert communications in the presence of a DRIS, whose random and time-varying reflective coefficients introduce FPJ. The DRIS-based FPJ not only impacts the covert communication between Alice and Bob but also decreases the detection error probabilities of the warden Willie, with neither Alice-Bob channel knowledge nor additional jamming power. To characterize the impact of the DRIS-based FPJ we design a detection rule for the warden Willie. We use the resulting false alarm rate (FAR) and missed detection rate (MDR) as monitoring performance metrics for Willie, and define the signal-to-jamming-plus-noise ratio (SJNR) as a communication performance metric for covert communications between Alice and Bob.
- To quantify the impact of the time-varying DRIS-based FPJ, the statistics of the DRIS-influenced channels are first derived. Based on the derived statistics and the designed detection rule, we then determine the detection threshold for the warden Willie to decide whether Alice and Bob are transmitting, considering the impact of the time-varying DRIS. Given the detection threshold, closed-form expressions for the FAR and MDR at Willie are derived. Furthermore, an asymptotic analysis of the

SJNR is conducted to demonstrate the impact of the DRIS-based FPJ on the communications between Alice and Bob. Simulation results are provided to validate the accuracy of the theoretical analyses.

- Based on the detailed theoretical analysis, we present unique properties of DRIS-based FPJ in covert communications. For example, the DRIS not only reduces the detection error probabilities at the warden Willie but also significantly disrupts the transmission between Alice and Bob, even when Willie experiences a missed detection. Increasing the transmit power at Alice does not significantly improve communication performance due to the DRIS. Instead, it exacerbates the impact of the DRIS-based FPJ on communications between Alice and Bob, and increases Alice’s risk of detection by the warden Willie. Moreover, a DRIS with only 1-bit quantized reflection coefficients is sufficient to enhance the detection accuracy at the warden and degrade the communication performance between Alice and Bob.

The rest of this paper is organized as follows. In Section II, we model covert communications in the presence of a DRIS, and the resulting impact on the wireless channels. Then, we define the FAR and MDR as performance metrics for Willie, and the SJNR as the performance metric for the covert transmissions between Alice and Bob. In Section III, we derive the statistics of the DRIS-based channels, and then we determine the detection threshold for the warden Willie to decide whether Alice and Bob are transmitting, taking into account the impact of the time-varying DRIS-based FPJ. Given the detection threshold, closed-form expressions for the FAR and MDR at the warden are derived. Moreover, an asymptotic analysis of the SJNR at Bob is conducted. In Section IV, the simulation and theoretical results are compared to validate the derived theoretical analyses and evaluate the impact of the DRIS. Finally, conclusions are given in Section IV.

*Notation:* We employ lowercase bold letters for a vector, e.g.,  $\mathbf{g}$ , and italic letters for a scalar, e.g.,  $N_D$ . The operators  $(\cdot)^T$  and  $(\cdot)^H$  respectively represent the transpose and the Hermitian transpose, and the symbol  $|\cdot|$  denotes the absolute value. Statistical expectation is indicated using  $\mathbb{E}[\cdot]$ .

## II. SYSTEM DESCRIPTION

In Section II-A, we first present the assumed covert communications scenario in the presence of a DRIS. Then, we model the wireless channels involved in Section II-B. In Section II-C, we describe the detection rule performed by the warden Willie to monitor the covert communications between Alice and Bob, and we define the FAR and MDR. In Section II-D, we define the SJNR as the communication performance metric used to evaluate the impact of the DRIS-based FPJ on the covert transmissions between Alice and Bob.

### A. Covert Communications in the Presence of a DRIS

Fig. 1 schematically illustrates a covert communication system in the presence of a DRIS. In covert communications, Alice aims to covertly transmit messages to Bob avoiding detection by the warden Willie. In this work, we investigate the

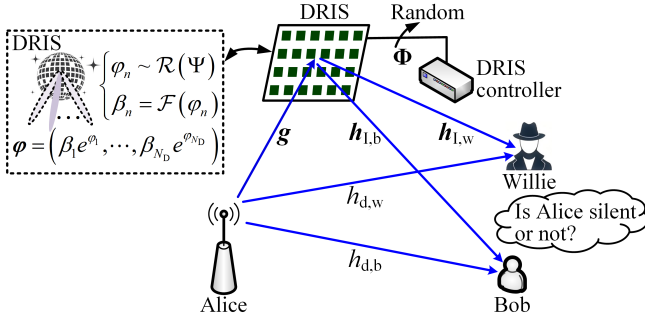


Fig. 1. Covert communications in the presence of a disco reconfigurable intelligent surface (DRIS), whose reflection coefficients are time-varying and random.

problem of determining the probability of Willie to correctly detect whether Alice and Bob are silent or not, without any coordination with them. Therefore, we assume that Willie has no channel state information for Bob, including his location.

To more accurately detect whether Alice is transmitting, the warden employs an  $N_D$ -element DRIS ( $N_D = N_{D,h} \times N_{D,v}$ ) with coefficients tuned by a simple programmable PIN [26]. The ON/OFF behavior of the PIN only allows for the implementation of discrete DRIS coefficients obtained by  $b$ -bit quantization of the reflection coefficient phase shifts and amplitudes. More specifically, the possible phase shifts and amplitudes of the DRIS are denoted as  $\Psi = \{\phi_1, \phi_2, \dots, \phi_{2^b}\}$  and  $\Omega = \{\alpha_1, \alpha_2, \dots, \alpha_{2^b}\}$ , respectively.

Similar to previous work in [34], [36]–[38], the reflection coefficients  $\varphi_n(t)$  and  $\beta_n(t)$  of the  $n$ -th DRIS element ( $n = 1, \dots, N_D$ ) are randomly generated and time-varying, and are assumed to be independent and identically distributed (i.i.d.) for different  $n$ . As a result, the passive beamforming of the DRIS can be expressed as  $\Phi(t) = \text{diag}(\varphi(t))$  where the DRIS reflection vector is denoted as  $\varphi(t) = [\beta_1(t)e^{j\varphi_1(t)}, \dots, \beta_{N_D}(t)e^{j\varphi_{N_D}(t)}]$ . In practice,  $\beta_n(t)$  is a function of  $\varphi_n(t)$ , i.e.,  $\beta_n(t) = \mathcal{F}(\varphi_n(t)) \in \Omega$  [20].

Based on the covert communication model in [4], [29], the  $m$ -th sample at the warden Willie over a given channel coherence interval can be expressed as

$$y_w(m) = \begin{cases} \underbrace{\frac{h_d^w s(m)}{\mathcal{L}^{\frac{\nu_d^w}{2}}}}_{\text{Direct link}} + \underbrace{\frac{h_D^w(m) s(m)}{\mathcal{L}^{\frac{\nu_g}{2}} \mathcal{L}^{\frac{\nu_1^w}{2}}}}_{\text{DRIS-Based link}} + n_w(m), & \text{transmitting,} \\ n_w(m), & \text{silent,} \end{cases} \quad (1)$$

where  $s(m)$  represents a covert symbol transmitted by Alice, and  $n_w(m)$  is additive white Gaussian noise (AWGN) with zero mean and variance  $\delta_w^2$ , i.e.,  $n_w(m) \sim \mathcal{CN}(0, \delta_w^2)$ . Similar to [5], [12], [13], we assume that the covert symbols transmitted by Alice follow the complex Gaussian distribution with zero mean and variance  $P_0$ , i.e.,  $s(m) \sim \mathcal{CN}(0, P_0)$ , where  $P_0$  is the transmit power at Alice.

In (1),  $h_d^w$  represents the direct channel between Alice and Willie, and  $h_D^w(m)$  denotes the cascaded DRIS-based channel

between Alice and Willie at the  $m$ -th sampling time. The cascaded DRIS-based channel  $h_D^w(m)$  can be expressed as

$$h_D^w(m) = \mathbf{g} \text{diag}(\varphi(m)) \mathbf{h}_1^w, \quad (2)$$

where  $\mathbf{g} \in \mathbb{C}^{1 \times N_D}$  denotes the channel between Alice and the DRIS, and  $\mathbf{h}_1^w \in \mathbb{C}^{N_D \times 1}$  denotes the channel between the DRIS and Willie. The factors  $\mathcal{L}^{\frac{\nu_d^w}{2}}$ ,  $\mathcal{L}^{\frac{\nu_g}{2}}$ , and  $\mathcal{L}^{\frac{\nu_1^w}{2}}$  represent the large-scale fading coefficients for  $h_d^w$ ,  $\mathbf{g}$ , and  $\mathbf{h}_1^w$  with corresponding path loss exponents of  $\nu_d^w$ ,  $\nu_g$ , and  $\nu_1^w$ , respectively. For ease of analysis, we assume that the locations of Alice and Willie are fixed, so that  $\mathcal{L}^{\frac{\nu_d^w}{2}}$ ,  $\mathcal{L}^{\frac{\nu_g}{2}}$ , and  $\mathcal{L}^{\frac{\nu_1^w}{2}}$  can be considered as approximately constant. In addition, we assume that Willie takes  $M \geq 2$  samples within the channel coherence time, resulting in the vector  $\mathbf{y}_w = [y_w(1), y_w(2), \dots, y_w(M)]^T$ .

The  $m$ -th signal sample received by Bob is given by

$$y_b(m) = \underbrace{\frac{h_d^b s(m)}{\mathcal{L}^{\frac{\nu_d^b}{2}}}}_{\text{Direct link}} + \underbrace{\frac{h_D^b(m) s(m)}{\mathcal{L}^{\frac{\nu_g}{2}} \mathcal{L}^{\frac{\nu_1^b}{2}}}}_{\text{DRIS-Based link}} + n_b(m), \quad (3)$$

where  $h_d^b$  denotes the direct channel between Alice and Bob,  $h_D^b(m)$  represents the cascaded DRIS-jammed channel between Alice and Bob at sample  $m$ , and  $n_b(m)$  is AWGN satisfying  $n_b \sim \mathcal{CN}(0, \delta_b^2)$ . In (3),  $\mathcal{L}^{\frac{\nu_d^b}{2}}$  and  $\mathcal{L}^{\frac{\nu_1^b}{2}}$  represent the large-scale fading coefficients for  $h_d^b$  and  $\mathbf{h}_1^b$ , respectively. The cascaded DRIS-jammed channel  $h_D^b(m)$  is expressed as

$$h_D^b(m) = \mathbf{g} \text{diag}(\varphi(m)) \mathbf{h}_1^b, \quad (4)$$

where  $\mathbf{h}_1^b \in \mathbb{C}^{N_D \times 1}$  denotes the channel between the DRIS and Bob.

## B. Channel Model

In this work, we consider a scenario where the DRIS is deployed close to Alice, while the warden Willie and Bob are positioned farther away. Therefore, the direct Alice- and Alice-Willie channels  $h_d^b$  and  $h_d^w$ , and the DRIS-Bob and DRIS-Willie channels  $\mathbf{h}_1^b$  and  $\mathbf{h}_1^w$  are modeled based on the far-field assumption, with elements that are assumed to be i.i.d. Gaussian random variables defined as [40].

$$h_d^b, h_d^w \sim \mathcal{CN}(0, 1), \quad (5)$$

$$\mathbf{h}_1^b, \mathbf{h}_1^w \sim \mathcal{CN}(\mathbf{0}_{N_D}, \mathbf{I}_{N_D}), \quad (6)$$

where  $\mathbf{0}_{N_D}$  is the  $N_D$ -dimensional zero vector and  $\mathbf{I}_{N_D}$  is the  $N_D$ -dimensional identity matrix.

The DRIS (and RIS in general) typically require a large number of reflective elements to mitigate the significant impact of multiplicative large-scale fading [34], [37], [38]. Therefore, the Alice-DRIS channel  $\mathbf{g}$  is generated based on a near-field model [41]:

$$\mathbf{g} = \sqrt{\frac{\varepsilon_g}{1 + \varepsilon_g}} \mathbf{g}^{\text{LOS}} + \sqrt{\frac{1}{1 + \varepsilon_g}} \mathbf{g}^{\text{NLOS}}, \quad (7)$$

where  $\varepsilon_g$  represents the Rician factor for  $\mathbf{g}$ . In (7), the elements of the non-line-of-sight (NLoS) component  $\mathbf{g}^{\text{NLOS}}$  follow

Rayleigh fading [40]. On the other hand, the elements of the line-of-sight (LoS) component  $\mathbf{g}^{\text{LOS}}$  are given by [41]

$$[\mathbf{g}^{\text{LOS}}]_r = e^{-j\frac{2\pi}{\lambda}(d_r - d_0)}, r = 1, \dots, N_D, \quad (8)$$

where  $\lambda$  is the wavelength of the covert signals,  $d_r$  and  $d_0$  represent the distance between Alice's antenna and the  $r$ -th DIRS element, and the distance between this antenna and the centre (origin) of the DIRS, respectively.

### C. Detection by Willie in the Presence of a DRIS

In covert communications, the warden Willie monitors the wireless channels to determine whether Alice and Bob are transmitting. In particular, Willie deduces from the samples in (1) which of the following two events has occurred: Alice and Bob are communicating ( $\mathcal{H}_1$ ), or Alice is silent ( $\mathcal{H}_0$ ). The following two error probabilities are widely used to measure the detection performance:  $\mathbb{P}(\mathcal{H}_1|\mathcal{H}_0)$ , which is the probability that Willie concludes Alice and Bob are communicating when they are not (the FAR), and  $\mathbb{P}(\mathcal{H}_0|\mathcal{H}_1)$ , which is the probability that Willie concludes Alice and Bob are silent when they are communicating (the MDR).

Since existing covert communication work relies almost entirely on the assumption that TDD channel reciprocity holds, the elements of the received sample vector  $\mathbf{y}_w$  are i.i.d. Consequently, Willie can use the total power of  $\mathbf{y}_w$  as a detection statistic to decide whether Alice and Bob are communicating [13], [16]–[19], [29], [32]. However, with the introduction of the DRIS, the basic assumption of channel reciprocity no longer applies. Consequently, the elements of the received sample vector  $\mathbf{y}_w$  are no longer i.i.d., even though they are received within the same channel coherence interval. The DRIS introduces the signal from an additional random and time-varying channel  $h_D^w(t)$  to the observation in (1), when Alice is transmitting to Bob.

To take into account the presence of the DRIS, Willie should use the following modified test statistic:

$$\mathcal{S} = \left\{ \mathbf{y}_w \mid \bigcup_{i_1 < \dots < i_N} \left( |y_w(i_1)|^2 \geq \varepsilon(i_1) \cap \dots \cap |y_w(i_N)|^2 \geq \varepsilon(i_N) \right) \right\}, \quad (9)$$

where  $1 \leq i_1 < \dots < i_N \leq M$ , and  $\varepsilon(m)$  denotes the detection threshold for the  $m$ -th component of the test. Based on (9), the detection made by the warden Willie can be expressed mathematically as

$$\mathcal{H}_1 : \mathbf{y}_w \in \mathcal{S}, \quad (10)$$

$$\mathcal{H}_0 : \mathbf{y}_w \notin \mathcal{S}. \quad (11)$$

Note that the time-varying detection thresholds  $\varepsilon(m)$ ,  $m = 1, \dots, M$  should be designed by considering the influence of the DRIS to ensure detection accuracy. The FAR and MDR are correspondingly expressed as

$$p_F = \mathbb{P}(\mathcal{H}_1|\mathcal{H}_0) = \mathbb{P}(\mathbf{y}_w \in \mathcal{S}|\mathcal{H}_0), \quad (12)$$

$$p_M = \mathbb{P}(\mathcal{H}_0|\mathcal{H}_1) = \mathbb{P}(\mathbf{y}_w \notin \mathcal{S}|\mathcal{H}_1). \quad (13)$$

### D. Signal-to-Interference-Plus-Noise Ratio at Bob

Based on (3), the received signals at Bob are subject to jamming by the DRIS due to  $h_D^b(t)$ . To characterize the impact of the DRIS on Bob, we use the SJNR defined by [38]

$$\eta_b = \frac{\frac{P_0 \mathbb{E}[|h_d^b s(m)|^2]}{\mathcal{L}^{\nu_d^b}}}{\frac{P_0 \mathbb{E}[|h_D^b(m)s(m)|^2]}{\mathcal{L}^{\nu_g} \mathcal{L}^{\nu_I^b}} + \delta_b^2}. \quad (14)$$

Consequently, the achievable rate at Bob is given by  $R_b = \log_2(1 + \eta_b)$ .

From (14), one can see that the covert transmissions between Alice and Bob are jammed by the time-varying DRIS, even though no jamming power is introduced, and Willie does not require CSI for Bob. In particular, due to the time-varying DRIS reflection coefficients  $\varphi(t)$ , the cascaded DRIS-jammed channel  $h_D^b(t) = \mathbf{g} \text{diag}(\varphi(t)) \mathbf{h}_1^b$  is time-varying even within the channel coherence time, causing the DRIS-jammed term  $h_D^b(m)s(m)$  to behave like ‘‘Gaussian noise’’. The vector  $\varphi(t)$  is randomly generated by Willie and is unknown to Alice and Bob. As a result, ACA interference<sup>1</sup> is introduced by breaking the channel reciprocity, which decreases the SJNR at Bob. This implies that the deployment of the DRIS by the warden Willie not only improves his detection performance but also degrades the communication performance between Alice and Bob.

## III. ASYMPTOTIC ANALYSIS OF COVERT COMMUNICATION PERFORMANCE

In Section III-A, the statistics of the DRIS-based channels are first derived to quantify the impact of the time-varying DRIS-based FPJ on covert communications. Then, we determine the detection threshold for the warden Willie to decide whether Alice and Bob are transmitting, considering the impact of the time-varying DRIS. In Section III-B, given the detection threshold, closed-form expressions for the detection error probabilities at Willie are derived. In Section III-C, an asymptotic analysis of the SJNR is conducted to illustrate the impact of the DRIS on the covert transmissions between Alice and Bob.

### A. Detection Error Probability in the Presence of a DRIS

In order to determine the detection thresholds in (9), we first derive the statistics of the cascaded DRIS-based channel  $h_D^w(t)$  between Alice and Willie.

*Proposition 1:* The random and time-varying DRIS-based channel  $h_D^w(t)$  converges in distribution to a complex Gaussian random variable as  $N_D \rightarrow \infty$ , i.e.,

$$\frac{h_D^w(t)}{\mathcal{L}^{\frac{\nu_g}{2}} \mathcal{L}^{\frac{\nu_d^w}{2}}} \xrightarrow{d} \mathcal{CN}\left(0, \frac{N_D \bar{\alpha}}{\mathcal{L}^{\nu_g} \mathcal{L}^{\nu_d^w}}\right), \quad (15)$$

where  $\bar{\alpha} = \mathbb{E}[|\beta_n(t)|^2] = \sum_{i=1}^{2^b} P_i \alpha_i^2$ , and  $P_i$  is the probability of the phase shift  $\varphi_r(t)$  taking the  $i$ -th value of

<sup>1</sup>The introduced ACA interference is different from interference due to channel aging (CA) [42], which arises from time variations in the RF propagation and computational delays between the time the channels are learned at the legitimate AP and when they are used for precoding.

$\Phi$ , i.e.,  $P_i = \mathbb{P}(\varphi_r(t) = \phi_i)$ . In this work, we assume that the discrete phases chosen at each DRIS element are uniformly distributed.

*Proof:* See Appendix A.  $\blacksquare$

To give the optimal detection threshold  $\varepsilon$  for Willie, the distribution of the Willie's received signal is derived. The  $m$ -th sample  $y_w(m)$  received at Willie under hypothesis  $\mathcal{H}_1$  is given by

$$y_w(m) = \frac{h_d^w s(m)}{\mathcal{L}^{\frac{\nu_d^w}{2}}} + \frac{h_D^w(m) s(m)}{\mathcal{L}^{\frac{\nu_g}{2}} \mathcal{L}^{\frac{\nu_w}{2}}} + n_w(m). \quad (16)$$

The direct channel  $h_d^w$  is constant over the channel coherence interval. Thus, based on Proposition 1, we have the following result:

$$c_w(m) = \frac{h_d^w}{\mathcal{L}^{\frac{\nu_d^w}{2}}} + \frac{h_D^w(m)}{\mathcal{L}^{\frac{\nu_g}{2}} \mathcal{L}^{\frac{\nu_w}{2}}} \stackrel{d}{\sim} \mathcal{CN}\left(\frac{h_d^w}{\mathcal{L}^{\frac{\nu_d^w}{2}}}, \frac{N_D \bar{\alpha}}{\mathcal{L}^{\nu_g} \mathcal{L}^{\nu_d^w}}\right). \quad (17)$$

However, in (16), the covert message  $s(m)$  also follows a complex Gaussian distribution, which is independent of  $c_w(m)$ . The product of two independent complex Gaussian variables is not Gaussian [43]. For two independent random variables  $X$  and  $Y$ , with probability density functions (PDFs)  $f_X(x)$  and  $f_Y(y)$ , respectively, the PDF of  $Z = XY$  can be computed using:

$$f_Z(z) = \int_{-\infty}^{+\infty} f_X(x) f_Y\left(\frac{z}{x}\right) \frac{1}{|x|} dx. \quad (18)$$

According to (18), the PDF of  $e_w(m) = c_w(m)s(m)$  is given by

$$\begin{aligned} f_{E_w}(e_w(m) | \mathcal{H}_1) &= \int_{-\infty}^{+\infty} \frac{1}{\frac{\pi N_D \bar{\alpha}}{\mathcal{L}^{\nu_g} \mathcal{L}^{\nu_d^w}}} e^{-\frac{\left|c_w(m) - \frac{h_d^w}{\mathcal{L}^{\frac{\nu_d^w}{2}}}\right|^2}{\frac{N_D \bar{\alpha}}{\mathcal{L}^{\nu_g} \mathcal{L}^{\nu_d^w}}}} \frac{1}{\pi P_0} e^{-\frac{|e_w(m)|^2}{P_0}} \left|\frac{1}{c_w(m)}\right|^2 dc_w(m) \\ &= \frac{4|e_w(m)|}{\frac{P_0 N_D \bar{\alpha}}{\mathcal{L}^{\nu_g} \mathcal{L}^{\nu_d^w}}} e^{-\kappa_e^2} \sum_{n=0}^{+\infty} \left(\frac{1}{n!}\right)^2 \left(\kappa_e^2 \frac{|e_w(m)|}{\frac{P_0 N_D \bar{\alpha}}{\mathcal{L}^{\nu_g} \mathcal{L}^{\nu_d^w}}}\right)^n K_n\left(\frac{2|e_w(m)|}{\sqrt{\frac{P_0 N_D \bar{\alpha}}{\mathcal{L}^{\nu_g} \mathcal{L}^{\nu_d^w}}}}\right), \end{aligned} \quad (20)$$

where  $\kappa_e$  is defined as  $\frac{|h_d^w|^2 \mathcal{L}^{\nu_g} \mathcal{L}^{\nu_d^w}}{N_D \bar{\alpha} \mathcal{L}^{\nu_d^w}}$  [43], and  $K_n(\cdot)$  represents the  $n$ -order modified Bessel function of the second kind.

Let  $Z$  and  $V$  be two independent random variables with PDFs  $f_Z(z)$  and  $f_V(v)$ , respectively. The PDF of  $W = Z + V$  is given by

$$f_W(w) = \int_{-\infty}^{+\infty} f_Z(z) f_V(w - z) dz. \quad (21)$$

In (16), the PDF of the AWGN  $n_w(m)$  can be expressed as

$$f_{N_w}(n_w(m)) = \frac{1}{\pi \delta_w^2} e^{-\frac{|y_w(m)|^2}{\delta_w^2}}. \quad (22)$$

Substituting (20) and (22) to (21), we have

$$\begin{aligned} f_{Y_w}(y_w(m) | \mathcal{H}_1) &= \int_{\mathcal{C}} f_{N_w}(y_w(m) - e_w(m)) f_{E_w}(e_w(m) | \mathcal{H}_1) de_w(m) \\ &= \int_{\mathcal{C}} \frac{1}{\pi \delta_w^2} e^{-\frac{|y_w(m) - e_w(m)|^2}{\delta_w^2}} \frac{2|e_w(m)|}{\pi \frac{P_0 N_D \bar{\alpha}}{\mathcal{L}^{\nu_g} \mathcal{L}^{\nu_d^w}}} K_0\left(\frac{|e_w(m)|}{\sqrt{\frac{P_0 N_D \bar{\alpha}}{\mathcal{L}^{\nu_g} \mathcal{L}^{\nu_d^w}}}}\right) de_w(m), \end{aligned} \quad (23)$$

where  $\int_{\mathcal{C}} \cdot$  represents an integral over the entire complex plane. However, it is difficult to compute the integral in (24) to obtain a closed-form expression.

The DRIS is controlled by the warden Willie, so he is aware of the value of  $\varphi(m)$  in  $h_D^w(m)$  at the  $m$ -th sampling time. Consequently, the conditional PDF of  $e_w(m)$  can be simplified from (20) to

$$\begin{aligned} f_{E_w}(e_w(m) | \mathcal{H}_1, h_D^w(m)) &\sim \mathcal{CN}(0, \delta_e^2(m)) \\ &= \frac{1}{\pi P_0 \left|\frac{h_d^w}{\mathcal{L}^{\frac{\nu_d^w}{2}}} + \frac{h_D^w(m)}{\mathcal{L}^{\frac{\nu_g}{2}} \mathcal{L}^{\frac{\nu_w}{2}}}\right|^2} \exp\left(-\frac{|e_w(m)|^2}{P_0 \left|\frac{h_d^w}{\mathcal{L}^{\frac{\nu_d^w}{2}}} + \frac{h_D^w(m)}{\mathcal{L}^{\frac{\nu_g}{2}} \mathcal{L}^{\frac{\nu_w}{2}}}\right|^2}\right). \end{aligned} \quad (25)$$

Conditioned on the fact that the sum of independent complex Gaussian random variables is also complex Gaussian, the conditional PDF of the received sample  $y_w(m)$  at Willie simplifies to

$$\begin{aligned} f_{Y_w}(y_w(m) | \mathcal{H}_1, h_D^w(m)) &\sim \mathcal{CN}(0, \delta_e^2(m) + \delta_w^2) \\ &= \frac{1}{\pi \left(\delta_w^2 + P_0 \left|\frac{h_d^w}{\mathcal{L}^{\frac{\nu_d^w}{2}}} + \frac{h_D^w(m)}{\mathcal{L}^{\frac{\nu_g}{2}} \mathcal{L}^{\frac{\nu_w}{2}}}\right|^2\right)} \exp\left(-\frac{|y_w(m)|^2}{\delta_w^2 + P_0 \left|\frac{h_d^w}{\mathcal{L}^{\frac{\nu_d^w}{2}}} + \frac{h_D^w(m)}{\mathcal{L}^{\frac{\nu_g}{2}} \mathcal{L}^{\frac{\nu_w}{2}}}\right|^2}\right). \end{aligned} \quad (26)$$

On the other hand, the PDF of the  $m$ -th sample  $y_w(m)$  received at Willie under hypothesis  $\mathcal{H}_0$  is equal to that of the AWGN:

$$f_{Y_w}(y_w(m) | \mathcal{H}_0) \sim \mathcal{CN}(0, \delta_w^2) = \frac{1}{\pi \delta_w^2} e^{-\frac{|y_w(m)|^2}{\delta_w^2}}. \quad (27)$$

Based on (26) and (27), we derive the detection thresholds  $\varepsilon(m)$  for (9) in the Proposition 2.

*Proposition 2:* For the detection in (10) and (11) performed by Willie, the optimal detection thresholds  $\varepsilon(m)$  ( $m = 1, \dots, M$ ) based on the likelihood ratio test (LRT) are given by

$$\begin{aligned} \varepsilon(m) &= \frac{\left(\delta_w^2 + P_0 \left|\frac{h_d^w}{\mathcal{L}^{\frac{\nu_d^w}{2}}} + \frac{h_D^w(m)}{\mathcal{L}^{\frac{\nu_g}{2}} \mathcal{L}^{\frac{\nu_w}{2}}}\right|^2\right) \delta_w^2}{P_0 \left|\frac{h_d^w}{\mathcal{L}^{\frac{\nu_d^w}{2}}} + \frac{h_D^w(m)}{\mathcal{L}^{\frac{\nu_g}{2}} \mathcal{L}^{\frac{\nu_w}{2}}}\right|^2} \times \\ &\quad \left(\ln\left(\delta_w^2 + P_0 \left|\frac{h_d^w}{\mathcal{L}^{\frac{\nu_d^w}{2}}} + \frac{h_D^w(m)}{\mathcal{L}^{\frac{\nu_g}{2}} \mathcal{L}^{\frac{\nu_w}{2}}}\right|^2\right) - \ln \delta_w^2\right). \end{aligned} \quad (28)$$

*Proof:* See Appendix B ■

According to Proposition 2, the introduction of the DRIS directly affects the detection thresholds  $\varepsilon(m)$  for the detection rule in (9). Without a DRIS, the detection thresholds in (28) reduce to the following fixed value:

$$\varepsilon = \frac{\left(\delta_w^2 + \frac{P_0|h_d^w|^2}{\mathcal{L}^{\nu_d^w}}\right)\delta_w^2}{\frac{P_0|h_d^w|^2}{\mathcal{L}^{\nu_d^w}}} \left( \ln\left(\delta_w^2 + \frac{P_0|h_d^w|^2}{\mathcal{L}^{\nu_d^w}}\right) - \ln \delta_w^2 \right). \quad (29)$$

### B. Error Probability Analysis of Willie's Detection

In this section, we quantify the impact of the time-varying DRIS-based FPJ on the decision-making process employed by the warden Willie. In particular, the theoretical FAR  $p_F$  and the MDR  $p_M$  are derived based on the detection thresholds  $\varepsilon(m)$  given by Proposition 2. We provide closed-form expressions for  $p_F$  and  $p_M$  in Theorem 1.

*Theorem 1:* The FAR and MDR can be expressed as

$$p_F = \mathbb{P}(\mathbf{y}_w \in \mathcal{S}|\mathcal{H}_0) \\ = \sum_{T=N}^M \sum_{i_1 < \dots < i_T} \left( \prod_{j=i_1}^{i_T} e^{-\frac{\varepsilon(j)}{\delta_w^2}} \prod_{i \neq i_1 \neq \dots \neq i_T} \left(1 - e^{-\frac{\varepsilon(i)}{\delta_w^2}}\right) \right), \quad (30)$$

and

$$p_M = \mathbb{P}(\mathbf{y}_w \notin \mathcal{S}|\mathcal{H}_1) \\ = \frac{\prod_{m=1}^M \left(1 - \exp\left(-\frac{\varepsilon(m)}{\delta_w^2 + \frac{P_0|h_d^w|^2}{\mathcal{L}^{\nu_d^w}} + \frac{P_0|h_D^w(m)|^2}{\mathcal{L}^{\nu_g} \mathcal{L}^{\nu_I^w}}}\right)\right)}{2^M} + \\ \sum_{T=1}^{N-1} \sum_{i_1 < \dots < i_T} \left( \prod_{j=i_1}^{i_T} \exp\left(\frac{-\varepsilon(j)}{\delta_w^2 + P_0 \left| \frac{h_d^w}{\mathcal{L}^{\frac{\nu_d^w}{2}}} + \frac{h_D^w(j)}{\mathcal{L}^{\frac{\nu_g}{2}} \mathcal{L}^{\frac{\nu_I^w}{2}}} \right|^2} \right) \times \right. \\ \left. \prod_{i \neq i_1 \neq \dots \neq i_T} \left(1 - \exp\left(-\frac{\varepsilon(i)}{\delta_w^2 + P_0 \left| \frac{h_d^w}{\mathcal{L}^{\frac{\nu_d^w}{2}}} + \frac{h_D^w(i)}{\mathcal{L}^{\frac{\nu_g}{2}} \mathcal{L}^{\frac{\nu_I^w}{2}}} \right|^2} \right)\right) \right). \quad (31)$$

*Proof:* See Appendix C ■

Based on Theorem 1, we can obtain important properties of the DRIS-based FPJ for covert communications. The larger the transmit power  $P_0$  at Alice, the smaller the FAR and MDR at Willie. In other words, increasing Alice's transmit power does not effectively improve the communication rate between Alice and Bob due to the DRIS-based FPJ. Instead, it increases the risk of detection by the warden Willie. Moreover, from (30) and (31), the improvement in FAR and MDR due to the use of the DRIS by Willie is independent of the specific values of the phase shifts of the DRIS. For example, only 1-bit quantized DRIS reflection coefficients are sufficient to enhance the detection accuracy at Willie.

### C. Communication Performance for Alice and Bob

The introduction of the DRIS by Willie not only improves his detection performance but also decreases quality of the covert transmissions between Alice and Bob. The time-varying DRIS can effectively jam the transmission between Alice and Bob even when Willie experiences a missed detection, since we see from (14) that there is an additional DRIS-based ACA interference that degrades Bob's reception performance. To mathematically characterize the impact of this interference, the ergodic SJNR at Bob derived in Theorem 2 below.

*Theorem 2:* The ergodic SJNR at Bob converges in distribution to

$$\eta_b = \frac{\frac{P_0}{\mathcal{L}^{\nu_d^b}}}{\frac{P_0 N_D \bar{\alpha}}{\mathcal{L}^{\nu_g} \mathcal{L}^{\nu_I^b}} + \delta_b^2}, \text{ as } N_D \rightarrow \infty. \quad (32)$$

*Proof:* See Appendix D ■

We see from Theorem 2 that increasing the transmit power does not result in an indefinite increase in the SJNR  $\eta_b$ . Instead,  $\eta_b$  asymptotically converges to a constant value  $\frac{\mathcal{L}^{\nu_g} \mathcal{L}^{\nu_I^b}}{\mathcal{L}^{\nu_d^b} N_D \bar{\alpha}}$  as  $P_0 \rightarrow \infty$ . However, based on Theorem 1, the FAR and MDR at Willie decrease rapidly as the Alice transmit power  $P_0$  increases. It is worth emphasizing here that the implementation of the DRIS relies on neither the CSI of the channels between Alice and Bob nor additional jamming power.

## IV. SIMULATION RESULTS AND DISCUSSION

In this section, we provide numerical results to demonstrate the impact of the DRIS on covert communication and evaluate the effectiveness of the theoretical analysis in Section III. Default settings for the simulation parameters are given below. As shown in Fig. 2, the single-antenna Alice is located at (0m, 0m, 5m), while the single-antenna Bob is randomly distributed within the ring-shaped region centered at (0m, 140m, 0m) with radii between 10m to 20m. The warden Willie is located at (0m, 100m, 0m) and monitors the covert communications between Alice and Bob assisted by a DRIS. The DRIS is equipped with 2048 ( $N_{D,h} = 64, N_{D,v} = 32$ ) reflective elements and deployed at  $(-d_{AD} \text{ m}, 0 \text{ m}, 5 \text{ m})$ , and the distance between Alice and the center of the DRIS i.e.,  $d_{AD}$  is nominally set to 1.5. The DRIS employs one-bit quantized phase shifts and amplitudes taken from  $\Psi = \{\frac{\pi}{9}, \frac{7\pi}{6}\}$  and  $\Omega = \mathcal{F}(\Theta) = \{0.8, 1\}$  [20], and the two phase shifts are chosen with equal probability. Consequently,  $\bar{\alpha}$  in Proposition 1 is calculated to be 0.82. We assume that the number of samples used for detection by Willie within the channel coherence time is  $M = 5$  and  $N = 2$  in the detection rule (9). The large-scale LoS and NLoS fading coefficients are defined in Table II based on the 3GPP propagation models [44], and the variance of the noise is  $\sigma_c^2 = -170 + 10 \log_{10}(BW)$  dBm with a transmission bandwidth of 180 kHz.

1) *Impact of Transmit Power at Alice:* Fig. 3 illustrates the FAR and MDR at Willie (left y-axis) versus the transmit power at Alice obtained from the following benchmarks: i) the simulated FAR without DRIS (FAR W/O DRIS) [5], [6] and ii) the corresponding theoretical FAR without DRIS, iii) the simulated FAR with DRIS (FAR W/ DRIS) and iv) the

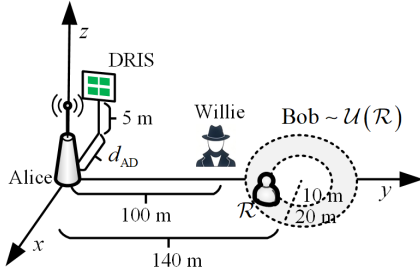


Fig. 2. An example of covert communications in the presence of a DRIS, where Bob is randomly located in the ring-shaped region  $\mathcal{R}$  centered at (0m, 140m, 0m) with a uniform distributed across radii between 10m to 20m, and Alice and the DIRS are deployed at (0 m, 0 m, 5m) and  $(-d_{AD}$  m, 0 m, 5m) respectively.

TABLE II  
WIRELESS CHANNEL SIMULATION PARAMETERS

| Large-scale Parameter | Value                        |
|-----------------------|------------------------------|
| LoS fading            | $35.6 + 22\log_{10}(d)$ (dB) |
| NLoS fading           | $32.6 + 36.7\log_{10}(d)$    |

derived theoretical FAR with DRIS in (30); v) the simulated MDR without DRIS (MDR W/O DRIS) [5], [6] and vi) the corresponding theoretical MDR without DRIS; vii) the simulated MDR with DRIS (MDR W/ DRIS) and viii) the derived theoretical MDR with DRIS in (31). The achievable rates at Bob (right y-axis) versus the transmit power at Alice are also presented in Fig. 3, comparing the following benchmarks: i) the simulated achievable rates without DRIS (Rate W/O DRIS) and ii) the theoretical achievable rates without DRIS; and iii) the simulated achievable rates with DRIS (Rate W/ DRIS) and iv) the theoretical achievable rates with DRIS in (32).

As illustrated in Fig. 3, the introduction of the DRIS by Willie significantly improves his FAR and MDR. Meanwhile, the DRIS significantly disrupts covert communications between Alice and Bob by launching FPJ attacks. It is worth noting that the implementation of DRIS by Willie requires neither the CSI of Alice-Bob channel nor additional jamming power. Moreover, Fig. 3 verifies the validity of Theorems 1 and 2, whose theoretical predictions match the results obtained from Monte Carlo simulations.

Both the detection improvement at Willie and the FPJ impact on covert communications increase with the transmit power at Alice, as shown in Fig. 3. We see that increasing the transmit power at Alice does not significantly improve covert communication performance due to the DRIS-based FPJ. Furthermore, as Alice increases the transmit power, the risk of being detected by the warden Willie becomes higher, while the covert communications between Alice and Bob suffers increased FPJ. In the following discussions, we investigate the impact of different factors on covert communications for both low and high transmit powers at Alice.

### 2) Impact of Number of DRIS Reflective Elements:

Fig. 4 illustrates the FAR and MDR at Willie (left y-axis), as well as the achievable rates at Bob (right y-axis) versus the number of DRIS elements for the different benchmarks. Results obtained for low transmit power (-7 dBm) and high

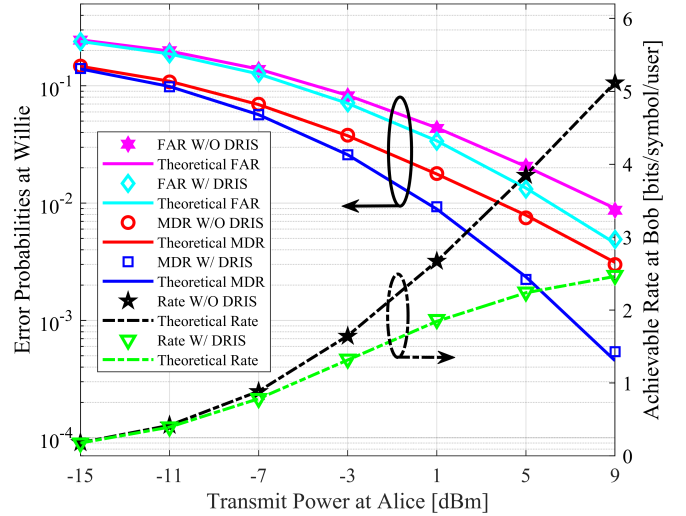


Fig. 3. Relationship between FAR and MDR and transmit power (left y-axis), and that between achievable rate and transmit power (right y-axis).

transmit power (5 dBm) are plotted in Figs. 4 (a) and (b), respectively. Consistent with Theorem 1, we observe that both the FAR and MDR decrease as the number of DRIS elements increases. Furthermore, we see that the rate of the decrease in the FAR and MDR is also influenced by the transmit power at Alice. Figs. 4 (a) and (b) also show that a higher transmit power at Alice leads to a higher detection accuracy at Willie.

Clearly, the impact of the DRIS becomes more pronounced as its number of elements increases. Figs. 4 (a) and (b) show that the achievable rates at Bob decrease with the number of DRIS reflective elements, and Willie can leverage a larger DRIS to reduce his detection error probabilities while at the same time degrading the covert transmissions between Alice and Bob. However, the rate of improvement in the FAR and MDR gradually decrease as the size of the DRIS continues to increase. Nevertheless, again consistent with Theorems 1 and 2, the detection errors at Willie and the achievable rate at Bob under DRIS-based FPJ degrade to zero as the number of DRIS elements approaches infinity.

3) *Impact of DRIS Reflection Coefficient Quantization:* In Fig. 5, the influence of quantization of the DRIS responses is investigated. A  $b$ -bit quantized DRIS with  $2^b$  phase shift values is modeled based on [45], where the phase shift values are denoted as  $\Psi = \{-\frac{\pi}{2}, -\pi + \frac{\pi}{2^{b-1}}, \dots, \frac{3\pi}{2} - \frac{\pi}{2^{b-1}}\}$ . Furthermore, based on [45], the time-varying phase shift and amplitude of the  $n$ -th DRIS element ( $n = 1, 2, \dots, N_D$ ) are modeled by

$$\begin{aligned} \beta_n(t) &= \mathcal{F}(\varphi_n(t)) \\ &= (1 - \alpha_{\min}) \left( \frac{\sin(\varphi_n(t) - \phi) + 1}{2} \right)^\mu + \alpha_{\min}, \end{aligned} \quad (33)$$

where  $\varphi_n(t) \in \Psi$  denotes the phase shift of the  $n$ -th DRIS element,  $\alpha_{\min} = \min\{\Omega\}$  represents the minimum DRIS amplitude, and  $\mu$  and  $\phi$  are constants determined by the specific RIS implementation. According to [45], we set  $\alpha_{\min} = 0.8$ ,  $\mu = 1.6$ , and  $\phi = 0$ .

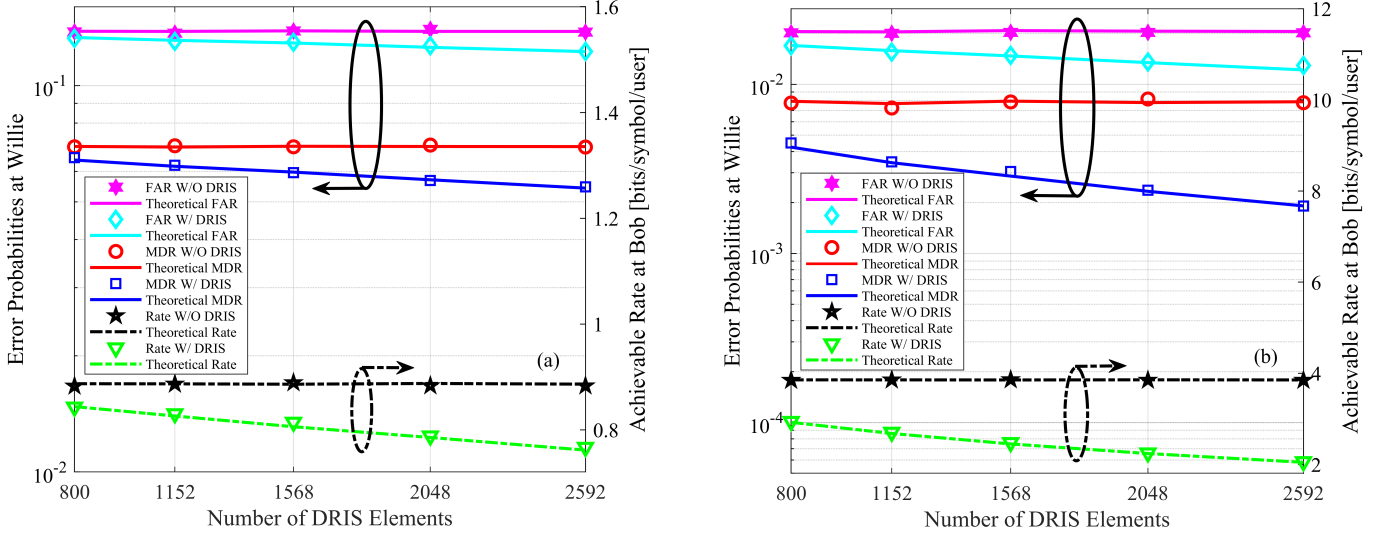


Fig. 4. FAR and MDR vs. the number of DRIS elements (left y-axis), and achievable rate vs. the number of DRIS elements (right y-axis) at (a) low transmit power (-7 dBm) and (b) high transmit power (5 dBm).

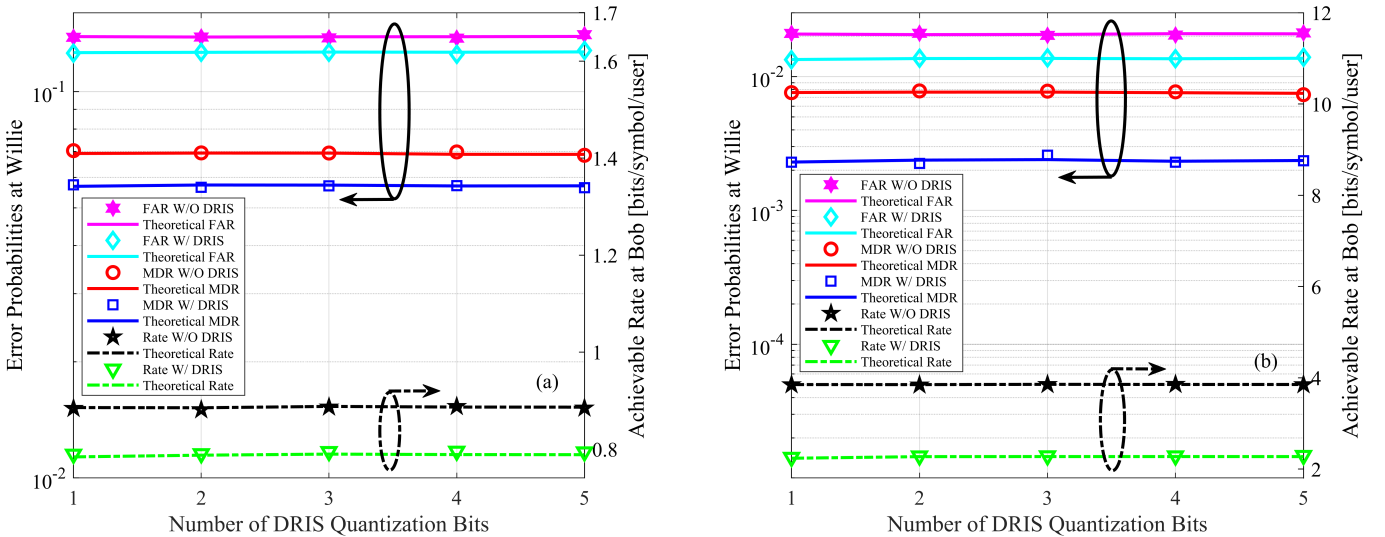


Fig. 5. FAR and MDR vs. the quantization resolution of the DRIS (left y-axis), and achievable rate vs. the quantization resolution of the of DRIS (right y-axis) at (a) low transmit power (-7 dBm) and (b) high transmit power (5 dBm).

In most RIS investigations, increasing the number of quantization bits typically results in a more significant impact. However, Fig. 5 presents a surprising result, showing that increasing the quantization resolution of the DRIS has only a minimal impact on the FAR and MDR at Willie and the achievable rate at Bob. This is because, according to Proposition 1, the statistics of the cascaded DRIS-based channels are not related to the specific choice of the DRIS reflection coefficients, but rather depend on the value of  $|\beta_n(t)|^2$ ,  $n = 1, \dots, N_D$ , i.e.,  $\bar{\alpha} = \mathbb{E}[|\beta_n(t)|^2] = \sum_{i=1}^{2^b} P_i \alpha_i^2$ . However, based on (33), increasing the number of DRIS quantization bits merely provides more available amplitude values for the DRIS without significantly increasing the value of  $\bar{\alpha}$ . As a result, a DRIS with higher quantization precision does not

lead to a more substantial impact on covert communications. Based on the results plotted in Figs. 4 and 5, a 1-bit DRIS with a large number of reflective elements is sufficient to enhance the detection accuracy at the warden Willie and degrade the covert transmissions between Alice and Bob.

4) *Impact of Distance Between Alice and DRIS:* According to Theorems 1 and 2, the impact of DRIS on covert communications is related to the large-scale fading of the cascaded DRIS-based channels  $h_D^w(t)$  and  $h_D^b(t)$ . Fig. 6 shows the FAR and MDR at Willie and the achievable rate at Bob as functions of the distance between Alice and DRIS  $d_{AD}$  for low and high transmit power levels, i.e., -7 dBm and 5 dBm transmit powers. We see that the impact of the DRIS on both detection performance at Willie and the achievable rate at Bob diminishes as  $d_{AD}$  increases. In other words, if the

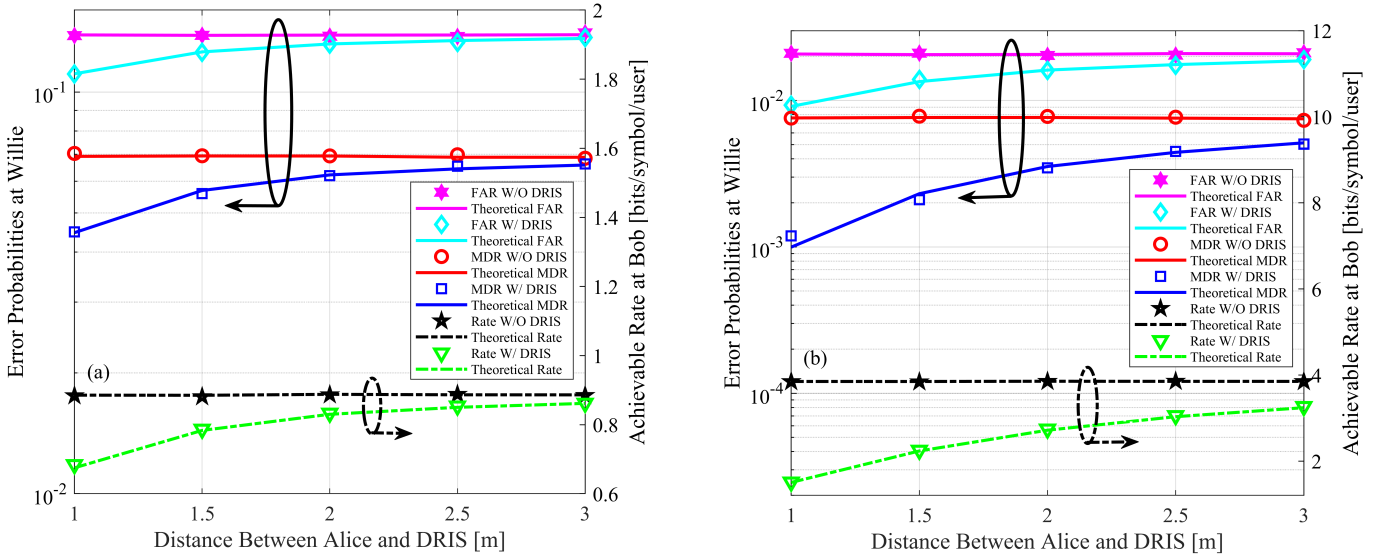


Fig. 6. FAR and MDR vs. the distance between Alice and DRIS (left y-axis), and achievable rate vs. the distance between Alice and DRIS (right y-axis) at (a) low transmit power (-7 dBm) and (b) high transmit power (5 dBm).

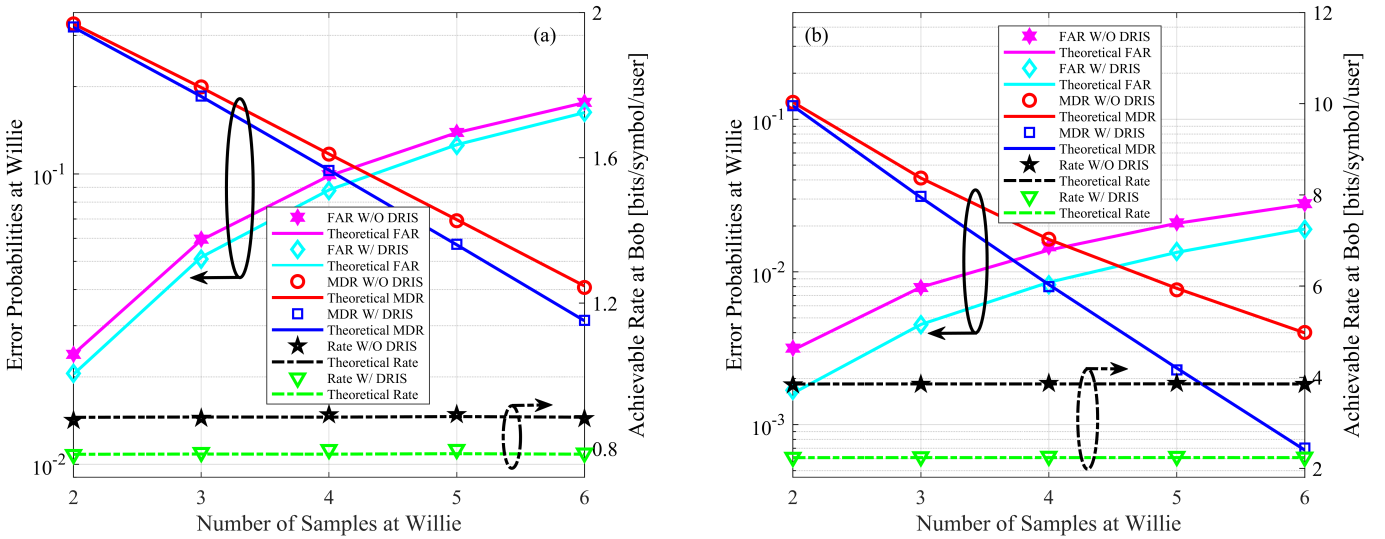


Fig. 7. FAR and MDR vs. the number of Willie's detections (left y-axis), and achievable rate vs. the number of Willie's detections (right y-axis) at (a) low transmit power (-7 dBm) and (b) high transmit power (5 dBm).

warden Willie aims to closely monitor covert communications between Alice and Bob and maximize the impact of the DRIS-based FPJ attacks, the DRIS should be deployed as close to Alice as possible.

5) *Impact of Number of Detection Samples*: Fig. 7 illustrates the relationship between the number of samples used for detection by Willie and achievable rate at Bob. While the number of samples has no impact on Bob's performance, it significantly impacts Willie's detection error probabilities, regardless of whether the DRIS is implemented.

We see that the MDR decreases monotonically with the number of Willie's detection samples, while the FAR increases. The results of Theorem 1 suggest that a trade-off between the FAR and MDR can be achieved by appropriately setting  $N$ . For example, when Willie makes six detections

within the channel coherence time, the parameter  $N$  in the detection rule can be changed from 2 to 3 to achieve a balance between the FAR and MDR.

## V. CONCLUSIONS

In this paper, we proposed a novel approach to help a warden Willie improve his ability to detect the presence of covert communications between Alice and Bob, while simultaneously jamming such communications. The proposed DRIS-based approach requires neither channel state information for the Alice-Bob channel nor active jamming power. The following conclusions can be drawn from the theoretical analysis and numerical results.

- 1) A DRIS with random and time-varying reflection coefficients introduces FPJ in covert communications. If the

detection rule performed by the warden Willie takes the time-varying DRIS-based FPJ into account, the DRIS not only reduces the FAR and MDR at Willie but also significantly disrupts the covert transmissions between Alice and Bob, even when Willie experiences a missed detection.

- 2) Increasing the transmit power at Alice does not significantly improve the communication performance between Alice and Bob due to the DRIS-based FPJ. Moreover, higher transmit power increases the detection accuracy at Willie. In addition, the covert communications between Alice and Bob experience more severe DRIS-based FPJ.
- 3) A 1-bit DRIS with a large number of reflective elements is sufficient to significantly improve the detection accuracy at the warden Willie and degrade the covert communication performance between Alice and Bob. Moreover, the warden Willie should deploy the DRIS as close to Alice as possible to effectively monitor the communications between Alice and Bob and maximize the impact of the DRIS-based FPJ attacks.

Our work demonstrates that illegitimate RISs can pose a significant threat to covert communications, even without relying on either channel knowledge or additional jamming power, highlighting a critical area of concern.

#### APPENDIX A PROOF OF PROPOSITION 1

Based on the definition of the cascaded DRIS-based channel between Alice and Willie expressed in (2), the cascaded DRIS-based channel  $h_D^w(t)$  can be written as

$$\frac{h_D^w(t)}{\mathcal{L}^{\frac{\nu_g^w}{2}} \mathcal{L}^{\frac{\nu_I^w}{2}}} = \sqrt{\frac{\varepsilon_g}{(\varepsilon_g + 1) \mathcal{L}^{\nu_g^w} \mathcal{L}^{\nu_I^w}}} \mathbf{g}^{\text{LOS}} \mathbf{h}_I^w \odot \varphi(t) + \sqrt{\frac{1}{(\varepsilon_g + 1) \mathcal{L}^{\nu_g^w} \mathcal{L}^{\nu_I^w}}} \mathbf{g}^{\text{NLOS}} \mathbf{h}_I^w \odot \varphi(t), \quad (34)$$

where  $\odot$  denotes the Hadamard product.

According to the definition of  $\mathbf{h}_I^w$  in (6) and the definition that  $\varphi(t) = [\beta_1(t)e^{j\varphi_1(t)}, \dots, \beta_{N_D}(t)e^{j\varphi_{N_D}(t)}]$ , we rewrite (34) as

$$\frac{h_D^w(t)}{\mathcal{L}^{\frac{\nu_g^w}{2}} \mathcal{L}^{\frac{\nu_I^w}{2}}} = \sqrt{\frac{\varepsilon_g \mathcal{L}^{\nu_g^w} \mathcal{L}^{\nu_I^w}}{(\varepsilon_g + 1) \mathcal{L}^{\nu_g^w} \mathcal{L}^{\nu_I^w}}} \sum_{r=1}^{N_D} \left( [\mathbf{g}^{\text{LOS}}]_r [\mathbf{h}_I^w]_r \beta_r(t) e^{j\varphi_r(t)} \right) + \sqrt{\frac{1}{(\varepsilon_g + 1) \mathcal{L}^{\nu_g^w} \mathcal{L}^{\nu_I^w}}} \sum_{r=1}^{N_D} \left( [\mathbf{g}^{\text{NLOS}}]_r [\mathbf{h}_I^w]_r \beta_r(t) e^{j\varphi_r(t)} \right). \quad (35)$$

The expectations of the variables in (35) are calculated as

$$\mathbb{E} \left[ [\mathbf{g}^{\text{LOS}}]_r [\mathbf{h}_I^w]_r \beta_r(t) e^{j\varphi_r(t)} \right] = 0, \quad (36)$$

$$\mathbb{E} \left[ [\mathbf{g}^{\text{NLOS}}]_r [\mathbf{h}_I^w]_r \beta_r(t) e^{j\varphi_r(t)} \right] = 0, \quad (37)$$

and their variances are given by

$$\text{Var} \left[ [\mathbf{g}^{\text{LOS}}]_r [\mathbf{h}_I^w]_r \beta_r(t) e^{j\varphi_r(t)} \right] = \mathbb{E} \left[ |[\mathbf{h}_I^w]_r|^2 \right] \mathbb{E} \left[ |\beta_r(t)|^2 \right], \quad (38)$$

$$= \sum_{i=1}^{2^b} P_i \alpha_i^2 = \bar{\alpha}, \quad (39)$$

and

$$\text{Var} \left[ [\mathbf{g}^{\text{NLOS}}]_r [\mathbf{h}_I^w]_r \beta_r(t) e^{j\varphi_r(t)} \right] = \mathbb{E} \left[ |[\mathbf{g}^{\text{NLOS}}]_r|^2 \right] \mathbb{E} \left[ |[\mathbf{h}_I^w]_r|^2 \right] \mathbb{E} \left[ |\beta_r(t)|^2 \right], \quad (40)$$

$$= \sum_{i=1}^{2^b} P_i \alpha_i^2 = \bar{\alpha}, \quad (41)$$

where  $P_i$  is the probability that the phase shift  $\varphi_r(t)$  takes the  $i$ -th value of  $\Phi$ , i.e.,  $P_i = \mathbb{P}(\varphi_r(t) = \phi_i), \forall r$ .

Since the number of DRIS elements is large, according to the Lindeberg-Lévy central limit theorem,  $\frac{h_D^w(t)}{\mathcal{L}^{\frac{\nu_g^w}{2}} \mathcal{L}^{\frac{\nu_I^w}{2}}}$  converges in distribution as follows:

$$\frac{h_D^w(t)}{\mathcal{L}^{\frac{\nu_g^w}{2}} \mathcal{L}^{\frac{\nu_I^w}{2}}} \xrightarrow{d} \mathcal{CN} \left( 0, \frac{N_D \bar{\alpha}}{\mathcal{L}^{\nu_g^w} \mathcal{L}^{\nu_I^w}} \right). \quad (42)$$

#### APPENDIX B PROOF OF PROPOSITION 2

According to (26) and (27), we can obtain the following LRT:

$$\rho = \frac{\delta_w^2}{\delta_w^2 + P_0 \left| \frac{h_d^w}{\mathcal{L}^{\frac{\nu_d^w}{2}}} + \frac{h_D^w(m)}{\mathcal{L}^{\frac{\nu_g^w}{2}} \mathcal{L}^{\frac{\nu_I^w}{2}}} \right|^2} \times \exp \left( - \frac{|y_w(m)|^2}{\delta_w^2 + P_0 \left| \frac{h_d^w}{\mathcal{L}^{\frac{\nu_d^w}{2}}} + \frac{h_D^w(m)}{\mathcal{L}^{\frac{\nu_g^w}{2}} \mathcal{L}^{\frac{\nu_I^w}{2}}} \right|^2} + \frac{|y_w(m)|^2}{\delta_w^2} \right) \quad (43)$$

Setting  $\rho = 1$ , we then have

$$|y_w(m)|^2 = \frac{\left( \delta_w^2 + P_0 \left| \frac{h_d^w}{\mathcal{L}^{\frac{\nu_d^w}{2}}} + \frac{h_D^w(m)}{\mathcal{L}^{\frac{\nu_g^w}{2}} \mathcal{L}^{\frac{\nu_I^w}{2}}} \right|^2 \right) \delta_w^2}{P_0 \left| \frac{h_d^w}{\mathcal{L}^{\frac{\nu_d^w}{2}}} + \frac{h_D^w(m)}{\mathcal{L}^{\frac{\nu_g^w}{2}} \mathcal{L}^{\frac{\nu_I^w}{2}}} \right|^2} \times \left( \ln \left( \delta_w^2 + P_0 \left| \frac{h_d^w}{\mathcal{L}^{\frac{\nu_d^w}{2}}} + \frac{h_D^w(m)}{\mathcal{L}^{\frac{\nu_g^w}{2}} \mathcal{L}^{\frac{\nu_I^w}{2}}} \right|^2 \right) - \ln \delta_w^2 \right). \quad (44)$$

Consequently, the optimal detection thresholds  $\varepsilon(m)$  for the detection rule in (9) can be obtained as in (28).

APPENDIX C  
PROOF OF THEOREM 1

We first derive the FAR in (30). When Alice and Bob are silent ( $\mathcal{H}_0$ ), the observations at Willie consist entirely of AWGN, i.e.,  $\mathbf{y}_w = [y_w(1), \dots, y_w(M)]^T = [n_w(1), \dots, n_w(M)]^T$ . Therefore, the modulus squared of the  $m$ -th sample  $|y_w(m)|^2$ , follows the exponential distribution with PDF

$$f_{|Y_w|^2}(y) = \frac{1}{\pi\delta_w^2} e^{-\frac{y}{\delta_w^2}}. \quad (45)$$

Consequently, the cumulative distribution function (CDF) of  $|y_w(m)|^2$  under  $\mathcal{H}_0$  can be expressed as

$$F_{|Y_w|^2}(y) = 1 - e^{-\frac{y}{\delta_w^2}}. \quad (46)$$

Under  $\mathcal{H}_0$ , the probability that there are only  $T$  samples with power greater than the detection thresholds in (28) is calculated as

$$\begin{aligned} p_T | \mathcal{H}_0 &= \mathbb{P}\left(|\mathbf{y}_w(i_1)|^2 \geq \varepsilon(i_1), \dots, |\mathbf{y}_w(i_T)|^2 \geq \varepsilon(i_T) | \mathcal{H}_0\right) \\ &= \sum_{i_1 < \dots < i_T} \left( \prod_{j=i_1}^{i_T} \mathbb{P}\left(|\mathbf{y}_w(j)|^2 \geq \varepsilon(j) | \mathcal{H}_0\right) \right. \\ &\quad \left. \prod_{i \neq i_1 \neq \dots \neq i_T} \mathbb{P}\left(|\mathbf{y}_w(i)|^2 < \varepsilon(i) | \mathcal{H}_0\right) \right), \end{aligned} \quad (47)$$

where  $1 \leq i_1 < \dots < i_T \leq M$ .

According to (45) and (46), the probability  $p_T | \mathcal{H}_0$  can be represented as

$$p_T | \mathcal{H}_0 = \sum_{i_1 < \dots < i_T} \left( \prod_{j=i_1}^{i_T} e^{-\frac{\varepsilon(j)}{\delta_w^2}} \prod_{i \neq i_1 \neq \dots \neq i_T} \left(1 - e^{-\frac{\varepsilon(i)}{\delta_w^2}}\right) \right). \quad (48)$$

The FAR of Willies detection test can be computed as

$$p_F = \sum_{T=N}^M p_T | \mathcal{H}_0. \quad (49)$$

Substituting (48) to (49), the FAR in (30) is obtained.

On the other hand, the MDR in (31) corresponds to the case where Alice and Bob are transmitting ( $\mathcal{H}_1$ ), but the warden Willie fails to detect the transmission. Based on (26),  $|y_w(m)|^2$  follows the exponential PDF given by

$$\begin{aligned} f_{|Y_w|^2}(y) &= \\ &= \frac{1}{\pi \left( \delta_w^2 + P_0 \left| \frac{h_d^w}{\mathcal{L}^{\frac{\nu_g}{2}}} + \frac{h_D^w(m)}{\mathcal{L}^{\frac{\nu_w}{2}} \mathcal{L}^{\frac{\nu_D}{2}}} \right|^2 \right)} \exp \left( \frac{-y}{\delta_w^2 + P_0 \left| \frac{h_d^w}{\mathcal{L}^{\frac{\nu_g}{2}}} + \frac{h_D^w(m)}{\mathcal{L}^{\frac{\nu_w}{2}} \mathcal{L}^{\frac{\nu_D}{2}}} \right|^2} \right). \end{aligned} \quad (50)$$

According to (50), the CDF of  $|y_w(m)|^2$  under  $\mathcal{H}_1$  can be expressed as

$$F_{|Y_w|^2}(y) = 1 - \exp \left( \frac{-y}{\delta_w^2 + P_0 \left| \frac{h_d^w}{\mathcal{L}^{\frac{\nu_g}{2}}} + \frac{h_D^w(m)}{\mathcal{L}^{\frac{\nu_w}{2}} \mathcal{L}^{\frac{\nu_D}{2}}} \right|^2} \right). \quad (51)$$

Under  $\mathcal{H}_1$ , the probability that there are only  $T$  samples with power greater than the detection thresholds in (28) is given by

$$p_T | \mathcal{H}_1 = \sum_{i_1 < \dots < i_T} \prod_{j=i_1}^{i_T} \exp \left( \frac{-\varepsilon(j)}{\delta_w^2 + \frac{P_0 |h_d^w|^2}{\mathcal{L}^{\nu_g}} + \frac{P_0 |h_D^w(j)|^2}{\mathcal{L}^{\nu_g} \mathcal{L}^{\nu_D}}} \right). \quad (52)$$

Consequently, the MDR for Willie's detection is calculated as

$$p_M = p_0 | \mathcal{H}_1 + \sum_{T=1}^{N-1} p_T | \mathcal{H}_1, \quad (53)$$

where

$$p_0 | \mathcal{H}_1 = \prod_{m=1}^M \left( 1 - \exp \left( - \frac{\varepsilon(m)}{\delta_w^2 + \frac{P_0 |h_d^w|^2}{\mathcal{L}^{\nu_g}} + \frac{P_0 |h_D^w(m)|^2}{\mathcal{L}^{\nu_g} \mathcal{L}^{\nu_D}}} \right) \right). \quad (54)$$

As a result, the MDR is derived, as given in (31).

APPENDIX D  
PROOF OF THEOREM 2

Similar to the conclusion of Proposition 1, the cascaded DRIS-jammed channel  $h_D^b(t)$  also converges in distribution to a complex Gaussian random variable as the number of DRIS elements grows large:

$$\frac{h_D^b(t)}{\mathcal{L}^{\frac{\nu_g}{2}} \mathcal{L}^{\frac{\nu_D}{2}}} \xrightarrow{d} \mathcal{CN} \left( 0, \frac{N_D \bar{\alpha}}{\mathcal{L}^{\nu_g} \mathcal{L}^{\nu_D}} \right), N_D \rightarrow \infty. \quad (55)$$

Conditioned on the fact the covert message  $s(m)$  and the DRIS-jammed channel are independent, the expectation in (14) can be reduced to

$$\mathbb{E} \left[ |h_D^b(m) s(m)|^2 \right] = \mathbb{E} \left[ |h_D^b(m)|^2 \right] \mathbb{E} \left[ |s(m)|^2 \right]. \quad (56)$$

Based on (55), the DRIS-based ACA interference in (14) converges in distribution to a fixed value

$$\mathbb{E} \left[ |h_D^b(m) s(m)|^2 \right] \xrightarrow{d} P_0 N_D \bar{\alpha}, \text{ as } N_D \rightarrow \infty. \quad (57)$$

Since  $h_d^b$  and  $s(m)$  are independent random variables, the expectation of  $|h_d^b s(m)|^2$  can be simplified to

$$\mathbb{E} \left[ |h_d^b s(m)|^2 \right] = \mathbb{E} \left[ |h_d^b|^2 \right] \mathbb{E} \left[ |s(m)|^2 \right]. \quad (58)$$

Based on the definition in (5), we have

$$\mathbb{E} \left[ |h_d^b s(m)|^2 \right] = P_0. \quad (59)$$

Substituting (57) and (59) to (14), the ergodic SJNR can be obtained as given in (32).

REFERENCES

- [1] A. Mukherjee, S. A. A. Fakoorian, J. Huang, and A. L. Swindlehurst, "Principles of physical layer security in multiuser wireless networks: A survey," *IEEE Commun. Surv. Tut.*, vol. 16, no. 3, pp. 1550–1573, 3rd Quarter 2014.
- [2] Y. Zou, J. Zhu, X. Wang, and L. Hanzo, "A survey on wireless security: Technical challenges, recent advances, and future trends," *Proceedings of the IEEE*, vol. 104, no. 9, pp. 1727–1765, Sep. 2016.

- [3] H. Pirayesh and H. Zeng, "Jamming attacks and anti-jamming strategies in wireless networks: A comprehensive survey," *IEEE Commun. Surv. Tut.*, vol. 24, no. 2, pp. 767–809, 2nd Quarter 2022.
- [4] X. Chen, J. An, Z. Xiong, C. Xing, N. Zhao, F. R. Yu, and A. Nallanathan, "Covert communications: A comprehensive survey," *IEEE Commun. Surv. Tut.*, vol. 25, no. 2, pp. 1173–1198, 2nd Quarter 2023.
- [5] B. A. Bash, D. Goeckel, and D. Towsley, "Limits of reliable communication with low probability of detection on AWGN channels," *IEEE J. Sel. Areas Commun.*, vol. 31, no. 9, pp. 1921–1930, Sept. 2013.
- [6] A. Abdelaziz and C. E. Koksul, "Fundamental limits of covert communication over MIMO AWGN channel," *Proc. IEEE CCNS*, Las Vegas, NV, Dec. 2017.
- [7] B. Yang, T. Taleb, G. Chen, and S. Shen, "Covert communication for cellular and X2U-enabled UAV networks with active and passive wardens," *IEEE Netw.*, vol. 36, no. 1, pp. 166–173, Feb. 2022.
- [8] S. Feng, X. Lu, S. Sun, and D. Niyato, "Mean-field artificial noise assistance and uplink power control in covert IoT systems," *IEEE Trans. Wireless Commun.*, vol. 21, no. 9, pp. 7358–7373, Sep. 2022.
- [9] O. A. Topal and G. Karabulut-Kurt, "Covert communication in cooperative NOMA networks," in *Proc. IEEE SIU*, Gaziantep, Turkey, Oct. 2020.
- [10] L. Tao, W. Yang, S. Yan, D. Wu, X. Guan, and D. Chen, "Covert communication in downlink NOMA systems with random transmit power," in *IEEE Wireless Commun. Lett.*, vol. 9, no. 11, pp. 2000–2004, Nov. 2020.
- [11] S. A. Ahmadzadeh and G. B. Agnew, "Turbo covert channel: An iterative framework for covert communication over data networks," in *Proc. IEEE INFOCOM*, Turin, Italy, Jul. 2013, pp. 2031–2039.
- [12] T. V. Sobers, B. A. Bash, S. Guha, D. Towsley, and D. Goeckel, "Covert communication in the presence of an uninformed jammer," *IEEE Trans. Wireless Commun.*, vol. 16, no. 9, pp. 6193–6206, Sept. 2017.
- [13] K. Li, P. A. Kelly, and D. Goeckel, "Optimal power adaptation in covert communication with an uninformed jammer," *IEEE Trans. Wireless Commun.*, vol. 19, no. 5, pp. 3463–3473, May 2020.
- [14] T.-X. Zheng, Z. Yang, C. Wang, Z. Li, J. Yuan, and X. Guan, "Wireless covert communications aided by distributed cooperative jamming over slow fading channels," *IEEE Trans. Wireless Commun.*, vol. 20, no. 11, pp. 7026–7039, Nov. 2021.
- [15] X. Chen, W. Sun, C. Xing, N. Zhao, Y. Chen, F. R. Yu, and A. Nallanathan, "Multi-antenna covert communication via full-duplex jamming against a warden with uncertain locations," *IEEE Trans. Wireless Commun.*, vol. 20, no. 8, pp. 5467–5480, Aug. 2021.
- [16] J. Hu, S. Yan, X. Zhou, F. Shu, J. Li, and J. Wang, "Covert communication achieved by a greedy relay in wireless networks," *IEEE Trans. Wireless Commun.*, vol. 17, no. 7, pp. 4766–4779, Jul. 2018.
- [17] M. Lin, C. Liu, and W. Wang, "Relay-assisted uplink covert communication in the presence of multi-antenna warden and uninformed jamming," *IEEE Trans. Commun.*, vol. 72, no. 4, pp. 2124–2137, Apr. 2024.
- [18] R. Sun, B. Yang, S. Ma, Y. Shen, and X. Jiang, "Covert rate maximization in wireless full-duplex relaying systems with power control," *IEEE Trans. Commun.*, vol. 69, no. 9, pp. 6198–6212, Sep. 2021.
- [19] J. Hu, K. Shahzad, S. Yan, X. Zhou, F. Shu, and J. Li, "Covert communications with a full-duplex receiver over wireless fading channels" in *Proc. IEEE Int. Commun. Conf. (ICC'18)*, Kansas City, MO, May 2018.
- [20] H. Zhang, S. Zeng, B. Di, Y. Tan, M. D. Renzo, M. Debbah, Z. Han, H. V. Poor, and L. Song, "Intelligent omni-surfaces for full-dimensional wireless communications: Principles, technology, and implementation," *IEEE Commun. Mag.*, vol. 60, no. 2, pp. 39–45, Feb. 2022.
- [21] C. Huang, S. Hu, G. C. Alexandropoulos, A. Zappone, C. Yuen, R. Zhang, M. Di Renzo, and M. Debbah, "Holographic MIMO surfaces for 6G wireless networks: Opportunities, challenges, and trends," *IEEE Wireless Commun.*, vol. 27, no. 5, pp. 118–125, Jul. 2020.
- [22] Q. Wu and R. Zhang, "Intelligent reflecting surface enhanced wireless network via joint active and passive beamforming," *IEEE Trans. Wireless Commun.*, vol. 18, no. 11, pp. 5394–5409, Nov. 2019.
- [23] Q. Wu, S. Zhang, B. Zheng, C. You, and R. Zhang, "Intelligent reflecting surface aided wireless communications: A tutorial," *IEEE Trans. Commun.*, vol. 69, no. 5, pp. 3313–3351, Jan. 2021.
- [24] S. Gong, X. Lu, D. T. Hoang, D. Niyato, L. Shu, D. I. Kim, Y.-C. Liang, "Toward smart wireless communications via intelligent reflecting surfaces: A contemporary survey," *IEEE Commun. Surv. Tut.*, vol. 22, no. 4, pp. 2283–2314, Fourth Quarter 2020.
- [25] R. Deng, B. Di, H. Zhang, Y. Tan, and L. Song, "Reconfigurable holographic surface-enabled multi-user wireless communications: Amplitude-controlled holographic beamforming," *IEEE Trans. Wireless Commun.*, vol. 21, no. 8, pp. 6003–6017, Aug. 2022.
- [26] T. Cui, M. Qi, X. Wan, J. Zhao, and Q. Cheng, "Coding metamaterials, digital metamaterials and programmable metamaterials," *Light-Sci. Appl.*, vol. 3, e218, Oct. 2014.
- [27] C. Huang, A. Zappone, G. C. Alexandropoulos, M. Debbah, C. Yuen, "Reconfigurable intelligent surfaces for energy efficiency in wireless communication," *IEEE Trans. Wireless Commun.*, vol. 18, no. 8, pp. 4157–4170, Jun. 2019.
- [28] C. Huang, R. Mo, and C. Yuen, "Reconfigurable intelligent surface assisted multiuser MISO systems exploiting deep reinforcement learning," *IEEE J. Sel. Areas Commun.*, vol. 38, no. 8, pp. 1839–1850, Aug. 2020.
- [29] L. Lv, Q. Wu, Z. Li, Z. Ding, N. Al-Dhahir, and J. Chen, "Covert communication in intelligent reflecting surface-assisted NOMA systems: Design, analysis, and optimization," *IEEE Trans. Wireless Commun.*, vol. 21, no. 3, pp. 1735–1750, Mar. 2022.
- [30] C. Wang, Z. Xiong, M. Zheng, N. Zhao, and D. Niyato, "Covert communications via two-way IRS with noise power uncertainty," *IEEE Trans. Commun.*, vol. 72, no. 8, pp. 4803–4815, Aug. 2024.
- [31] Y. Wu, X. Chen, M. Liu, L. Xu, N. Zhao, X. Wang, and D. W. Kwan Ng, "IRS-assisted covert communication with equal and unequal transmit prior probabilities," *IEEE Trans. Commun.*, vol. 72, no. 5, pp. 2897–2912, May 2024.
- [32] C. Wang, X. Chen, J. An, Z. Xiong, C. Xing, N. Zhao, and D. Niyato, "Covert communication assisted by UAV-IRS," *IEEE Trans. Commun.*, vol. 71, no. 1, pp. 357–369, Jan. 2023.
- [33] Q. Wang, S. Guo, C. Wu, C. Xing, N. Zhao, D. Niyato, and G. K. Karagiannis, "STAR-RIS aided covert communication in UAV air-ground networks," *IEEE J. Sel. Areas Commun.*, vol. 43, no. 1, pp. 245–258, Jan. 2025.
- [34] H. Huang, L. Dai, H. Zhang, C. Zhang, Z. Tian, Y. Cai, A. L. Swindlehurst, and Z. Han, "DISCO might not be funky: Random intelligent reflective surface configurations that attack," *IEEE Wireless Commun.*, vol. 31, no. 5, pp. 76–82, Oct. 2024.
- [35] H. Wang, Z. Han and A. L. Swindlehurst, "Channel reciprocity attacks using intelligent surfaces with non-diagonal phase shifts," *IEEE Open J. Commun. Soc.*, vol. 5, pp. 1469–1485, Feb. 2024.
- [36] H. Huang, Y. Zhang, H. Zhang, C. Zhang, and Z. Han, "Illegal intelligent reflecting surface based active channel aging: When jammer can attack without power and CSI," *IEEE Trans. Veh. Technol.*, vol. 72, no. 8, pp. 11018–11022, Aug. 2023.
- [37] H. Huang, Y. Zhang, H. Zhang, Y. Cai, A. L. Swindlehurst, and Z. Han, "Disco intelligent reflecting surfaces: Active channel aging for fully-passive jamming attacks," *IEEE Trans. Wireless Commun.*, vol. 23, no. 1, pp. 806–819, Jan. 2024.
- [38] H. Huang, L. Dai, H. Zhang, Z. Tian, Y. Cai, C. Zhang, A. L. Swindlehurst, and Z. Han, "Anti-jamming precoding against disco intelligent reflecting surfaces based fully-passive jamming attacks," *IEEE Trans. Wireless Commun.*, vol. 23, no. 8, pp. 9315–9329, Aug. 2024.
- [39] G. Li, P. Staat, H. Li, M. Heinrichs, C. Zenger, R. Kronberger, H. Elders-Boll, C. Paar, A. Hu, "RIS-jamming: Breaking key consistency in channel reciprocity-based key generation," *IEEE Trans. Inf. Forensics Secur.*, vol. 19, pp. 5090–5105, Apr. 2024.
- [40] D. Tse and P. Viswanath, *Fundamentals of Wireless Communication*. Cambridge Univ. Press, Cambridge, U.K., 2005.
- [41] M. Cui and L. Dai, "Channel estimation for extremely large-scale MIMO: Far-field or near-field?" *IEEE Trans. Commun.*, vol. 70, no. 4, pp. 2663–2677, Apr. 2022.
- [42] K. T. Truong and R. W. Heath Jr., "Effects of channel aging in massive MIMO systems," *J. Commun. Netw.-S. Kor.*, vol. 15, no. 4, pp. 338–351, Aug. 2013.
- [43] N. O'Donoghue and J. M. F. Moura "On the product of independent complex Gaussians," *IEEE Trans. Signal Process.*, vol. 60, no. 3, pp. 1050–1063, Mar. 2012.
- [44] Further Advancements for E-UTRA Physical Layer Aspects (Release 9), document 3GPP TS 36.814, Mar. 2010.
- [45] S. Abeywickrama, R. Zhang, Q. Wu, C. Yuen, "Intelligent reflecting surface: Practical phase shift model and beamforming optimization," *IEEE Trans. Commun.*, vol. 68, no. 9, pp. 5849–5863, Sept. 2020.